CrossMark

Orientation Dependent Compressive Response of Human Femoral Cortical Bone as a Function of Strain Rate

Tusit Weerasooriya[1] · Brett Sanborn[2,3] · C. Allan Gunnarsson[1] · Mark Foster[2]

Abstract Under extreme environments, such as a blast or impact event, the human body is subjected to high-rate loading, which can result in damage such as torn tissues and broken bones. The ability to numerically simulate these events would help improve the design of protective gear by iterating different configurations of protective equipment to reduce injuries. Computer codes capable of simulating these events require accurate rate-dependent material models representing the material deformation and failure (or injury) to properly predict the response of human body during simulation. Therefore, the high-rate material response must be measured to allow for simulation of high-rate events. This study seeks to quantify the high-rate mechanical response of human femoral cortical bone for use in high fidelity human anatomical models. Cortical bone compression specimens were extracted from the longitudinal and transverse directions relative to the long axis of the femur from three male donors, ages 36, 43, and 50. The compressive behavior of the cortical bone was studied at quasi-static (0.001/s), intermediate (1/s), and dynamic (~1000/s) strain rates using a split-Hopkinson pressure bar to determine the strain rate dependency and anisotropic effect on the strength of bone. The results indicate that cortical bone is anisotropic and stronger in the longitudinal direction compared to the transverse direction.

The human cortical bone compressive response was also rate dependent in both directions, demonstrating significant increase in strength with increase in strain rate. Additionally, as the strain rate increased from intermediate to dynamic, a decrease in the elongation at transverse orientation was observed, which would indicate the bone becomes more brittle.

Keywords Cortical · Image correlation · Compression · Orientation · Femur · High Rate · Dynamic behavior

Introduction

Human long bone has a complex hierarchical structure organized at a variety of length scales, as shown in Fig. 1. At the nano-scale, cortical bone is comprised of collagen and hydroxyapatite crystals. At the micro-scale, these constituents organize into mineralized collagen fibrils. Fiber arrays are further organized into a lamellar. Cylindrical structures (Haversian structure) of multiple concentric lamellae surrounding central blood vessel (Haversian canal) are osteons. These cylindrical osteons are about 200 μm in diameter [1] and their long axes are oriented parallel to the longitudinal axis of long bones, such as the femur, tibia, fibula, etc. This orientation of osteons creates an anisotropic mechanical response such that cortical bone demonstrates different properties based on orientation. This anisotropy must be understood and incorporated into material models to properly represent the deformation behavior. Several studies on bone have been conducted to study the fracture behavior at the micro-scale during quasi-static loading [2, 3]. The fracture behavior of human bone has also been investigated at high loading rate [4–6]. In addition to fracture response, understanding the anisotropic
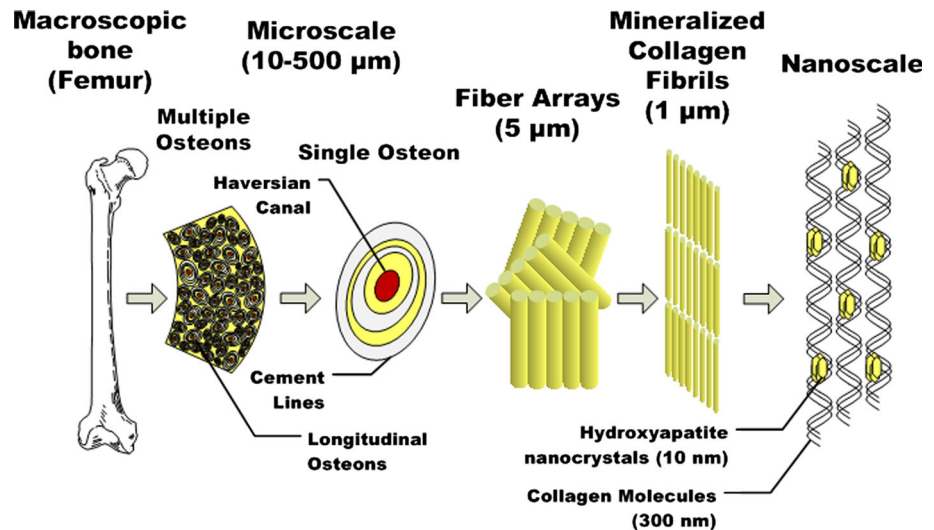
✉ Tusit Weerasooriya
  tusit.weerasooriya.civ@mail.mil; tusitw_j@me.com

[1] US Army Research Laboratory (ARL),
   Aberdeen Proving Ground, MD, USA

[2] ORISE/US Army Research Laboratory,
   Aberdeen Proving Ground, MD, USA

[3] Present Address: Sandia National Laboratory, Albuquerque,
   NM, USA

Fig. 1 Hierarchical structure of cortical bone

compressive response of bone is critical for building accurate material models.

McElhaney [7] first investigated the strain rate dependence of human cortical bone in compression. The high-rate properties were studied using a piezoelectric load cell and compressed gas powered piston system up to strain rates of 1500/s. He found that bone was viscoelastic and rate dependent in compression, increasing in stiffness and strength with increased strain rate. His study used embalmed bone; others have shown that the ultimate strength, maximum strain, and elastic modulus measurements made on embalmed bone do not represent the non-embalmed in vitro bone response [8], and that the level of formalin concentration in the storage fluid affects the material properties of the bone [9]. In addition, high rate loading experimentation is complex; it is vital to understand the specimen stress state during the transmission of the loading stress wave. The specimen could be experiencing varying stress states during the experiment if the loading stress pulse is not properly shaped. During the last half century, high rate experimentation has improved, making modern high rate experimental data more reliable. A major goal of the current study was to improve the understanding of the strain rate dependent mechanical response of bone. This was achieved by examining the rate-dependent compressive properties of bone that had not been embalmed using modern high loading rate experimental methods. In addition, direct in situ measurement of specimen strain was performed using a novel optical method [10].

The split-Hopkinson pressure bar (SHPB) experimental method has been used to study the rate dependence of animal cortical bone. Tennyson et al. [11] studied bovine femur over a strain rate range of 10 to 450/s and developed a linear viscoelastic model describing the mechanical

behavior. Stress and strain measurements were calculated using typical SHPB wave mechanics. Lewis and Goldsmith [12, 13] developed a biaxial method to test bovine bone under simultaneous compression and torsion, and also under compression, tension, and torsion separately. They used strain gages bonded directly to the surface of the bone specimens for more accurate strain measurements. They found that the pre-fracture response of bovine bone in compression was viscoelastic, and the compressive response increased with strain rate. Additionally, the bone accumulated residual permanent strain after load removal prior to fracture in combined torsion and compression. This deformation mechanism was not observed for uniaxial compression.

Unfortunately, bone specimens need to be dried for proper strain gage adhesion. This drying process has been shown to alter the mechanical response of bone due to the hydration-dependent behavior of bone collagen [14, 15]. Katsamanis et al. [16] studied the effect of loading rate on the elastic modulus and Poisson's ratio of human femoral cortical bone using one-dimensional wave theory and strain gages bonded to the surface of the bone in two directions at multiple locations. The experiments were conducted by impacting small steel balls longitudinally on the bone specimens. The Young's modulus of the bone increased from 16.2 GPa at quasi-static rates to 19.9 GPa at dynamic rates. None of these studies investigated the effect of bone's microstructural anisotropy on the mechanical response.

Tanabe et al. [17] studied the anisotropy of bovine femur and the effect of strain rate up to 100/s. The elastic modulus was found to be strongly dependent on the loading orientation of the bone with the elastic modulus in the longitudinal direction more than double that of the transverse direction. The cortical bone elastic moduli were

76

J. dynamic behavior mater. (2016) 2:74–90

similar in both the radial and tangential directions. Adharapurapu et al. [18] investigated the rate dependency and orientation dependency of fracture properties and compressive behavior of bovine cortical bone. Similar to what was previously reported, the bone's mechanical response was found to be anisotropic, with the longitudinal specimens about 50 % stronger than the transverse orientation. Both the strength and stiffness of the bovine bone increased from quasi-static to high loading rate, while the elongation decreased. Recently, Cloete et al. [19] and Bekker et al. [20] also studied the rate dependent response of bovine femur using the Hopkinson bar method. The strain rate of their studies ranged from 0.0001 to 1000/s. In these studies, they kept the strain rate constant by using a tapered striker. Their results show that the stress–strain response fell into two distinct concentrations based on the strain rate: the response was similar for all experiments conducted at 0.0001–0.1/s, while a different higher response was reported for experiments conducted in the range of 250–1000/s. Gunnarsson et al. [4] and Sanborn et al. [5] studied the anisotropic fracture response of human femur cortical bone. They found that the fracture toughness depended on the loading rate. Shannahan et al. [6] were able to quantify the loading rate dependent deviation of the fracture process from Mode I tensile to Mode II shear, due to bone anisotropy.

In contrast, Ferreira et al. [21] studied bovine cortical bone at high strain rate using a SHPB apparatus and did not find statistically different results for the compressive strength of longitudinal or transverse specimens. However, the validity of their results may be questionable due to an absence of dynamic equilibrium during their experimentation. Lee and Park [22] found qualitative evidence of anisotropy, in agreement with Adharapurapu et al. [18] using the SHPB technique; however, their experiments also did not achieve specimen dynamic equilibrium, necessary as outlined by Chen and Song [23]. Similarly, Kulin et al. [24] studied the effect of loading rate and age on the failure and compressive behavior of equine cortical bone and found it to be strain rate dependent and anisotropic. They found that the longitudinal direction was both stronger and stiffer at all loading rates compared to transverse specimens, with strength and stiffness increasing as strain rate increased. Porcine cortical femur and skull bone has also been investigated at high rates [25, 26].

The microstructure of human bone found in long bones is osteonal with a Haversian structure, whereas the microstructure of porcine and bovine bones has a plexiform structure [17, 27, 28]. Haversian structure is typified by canals that run at the center of the osteon along its axis and are surrounded by concentric lamellae. Conversely, plexiform bone is found in animals that reach maturity quickly and is characterized by a brick-like structure that is formed from mineral buds that grow first perpendicular and then parallel to the outer bone surface [27]. Parts of bovine femur may have a Haversian microstructure, while other parts may have a plexiform structure [28]. Since plexiform bone is rarely found in humans, the dynamic mechanical behavior obtained through experimentation on animal bones may not accurately represent the behavior of human bone with a different microstructure. Therefore, it is important that mechanical response studies are conducted with human bones, ensuring accurate material models.

Aside from the work of Lewis and Goldsmith [12, 13], previous research [18, 22, 24] used traditional SHPB assumptions to measure specimen strain or fracture response. Bone fails at relatively small strains and can be modeled as an elastic material similar to brittle materials, such as ceramics. This small strain to failure makes measurement of strain very important, which is difficult using a far-field technique such as machine displacement or bar signal analysis [23]. A non-traditional non-contact digital image correlation (DIC) method was used in this study to measure the specimen strain at all strain rates, thus avoiding issues associated with bar signal noise, as well as test machine compliance during the lower loading rate experiments. To the authors' knowledge, this is the first study to investigate the rate dependent mechanical compressive response of wet, un-embalmed human femoral cortical bone in two orientations using in situ strain measurement with high rate experiments performed at dynamic equilibrium and constant strain rate conditions.

Experiments

Material

Cortical bone samples were extracted from the femur diaphysis (shown in Fig. 2) of three male cadavers, ages 36, 43, and 50. Samples were extracted from the anterior, posterior, medial, and lateral regions along the diaphysis. The location of each specimen was carefully recorded. Nominal dimensions of the cube-shaped samples were $3 \times 3.25 \times 4$ mm. The gage lengths of the longitudinal (long) and transverse (trans) specimens were 3.22 ± 0.08 mm and 2.96 ± 0.125 mm, respectively. The cortical bone samples were stored refrigerated (1–4 °C) in Hank's Buffered Salt Solution (HBSS) after fabrication and prior to testing to preserve the microstructure and mechanical properties [29]. A total of 71 experiments were conducted for samples taken from directions longitudinal and transverse to the osteon direction in the bone. Table 1 shows the breakdown of the number of individual samples used at each loading rate and direction. Roughly the same number of samples from each donor at each rate was used

Fig. 2 Cortical bone specimens were extracted from the diaphysis and loading orientations with respect to osteon (long bone axis) direction
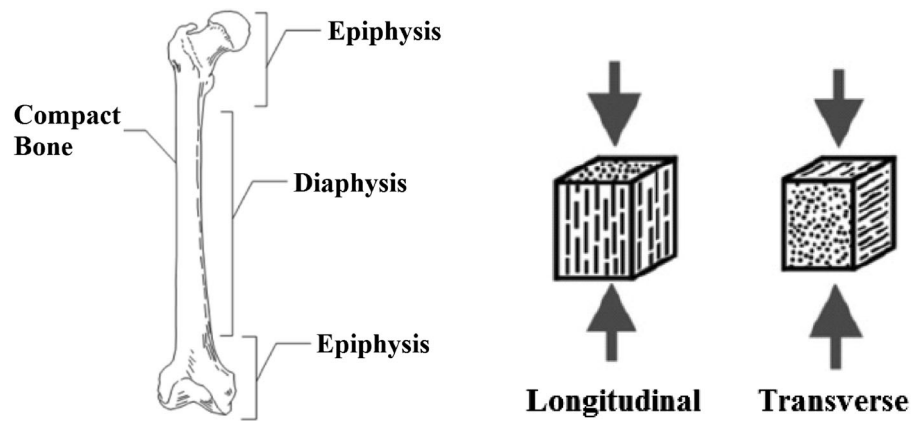
Table 1 Number of experiments in each loading direction for each strain rate

	Transverse direction	Longitudinal direction
Quasi-static rate (~ 0.001/s)	12	12
Intermediate rate (~ 1/s)	11	11
High rate (~ 1000/s)	14	11

to obtain an average behavior of cortical bone in uniaxial compression.

Strain Measurements

In these experiments, strain was measured on the surface of the specimen using optical digital image correlation (DIC) by analyzing the images of the speckled specimen surface acquired during the experiment. Initially the DIC software computed the Lagrange strain tensor; the Lagrange strain tensor was then converted to true (or log) strain for all experiments. All strain data reported here are true strains unless otherwise noted. To use DIC, images of the speckled specimen surface were recorded using different cameras based on the strain rate of the experiment. At the quasi-static rate, Point Grey Research Grasshopper cameras were used at a frame rate of 1 fps and a resolution of 2048 by 2048 pixels. At the intermediate rate, a Photron APX-RS high-speed camera was used at a frame rate of 1000 fps and a resolution of 1024 by 1024 pixels. At the dynamic rate, a Shimadzu HPV-2 with a resolution of 312 by 260 pixels was used at a frame rate of 500 K fps.

At the dynamic rate, bar strain pulses were recorded using a high speed (100 MHz) digital oscilloscope using differential inputs to measure voltage change in half-bridge Wheatstone bridge circuits connected to diametrically opposite mounted strain gages on the incident and transmission bars. The oscilloscope was triggered using a pulse width trigger at the end of the incident pulse; the oscilloscope provided a synchronized trigger-out that fired the high power flash and also initiated the recording of the HPV-2 ultra high speed camera. The camera provided an event signal to the oscilloscope for each picture, which allowed for the camera images to be synced to the strain gage data.

Quasi-Static and Intermediate Rate Experiments

An Instron load frame in displacement control was used for quasi-static (approximately 0.001/s) and intermediate (approximately 1/s) rate experiments. The bone specimen strain was measured using DIC [30–33]. The strain rate was calculated for each specimen using the linear slope of the strain history and was approximately constant from start of loading to until the specimen starts to fail at the maximum load. This technique avoids problems such as alignment of the strain gage relative to the loading axis and other typical limiting factors such as the maximum strain of the gage. DIC provides a full-field strain map on the specimen for each data point (picture); in contrast, a strain gage provides only a single data point, without any insight as to the level of strain uniformity along the specimen during the experiment. For DIC, a high contrast speckle pattern is applied to the specimen surface. Cameras, of various speeds based on the strain rate, recorded pictures of the speckle pattern on the surface of the specimen during compression. During post-processing, the DIC software computes the change in shape and location of the speckle pattern using pixel gray level values. This optical pattern tracking allows for measurement of surface deformation

78

J. dynamic behavior mater. (2016) 2:74–90

and strain tensors, while accounting for rigid body displacements. For these bone specimens, a light mist of matte black paint was applied to the already light color of the bone to create the speckle pattern.

High Rate Experiments

High rate compression experiments were conducted using a SHPB setup (Fig. 3). The setup, made of aluminum, consisted of a solid 19.05-mm diameter incident bar with resistive strain gages and a hollow transmission bar (tube) with an outer diameter of 19.05 mm and an inner diameter of 16.17 mm. The transmission bar used semiconductor strain gages to improve the signal to noise ratio of the weak transmitted signal. The engineering stress σ_s is calculated using [23]

$$\sigma_s(t) = (A_t/A_s)E\varepsilon_T(t) \tag{1}$$

where A_t and A_s are the cross-sectional areas of the transmission bar and specimen, respectively. E is the Young's modulus of the bar material, while ε_T is the strain measured from the transmission bar. Since a hollow transmission bar was used, the strain rate is calculated using [34]

$$\dot{\varepsilon} = \frac{c_0}{L_s}\left[\left(1 - \frac{A_i}{A_t}\right)\varepsilon_i(t) - \left(1 + \frac{A_i}{A_t}\right)\varepsilon_r(t)\right]. \tag{2}$$

where c_0 is the wave speed of the bar material and L_s is the length of the sample. A_i and A_t are the cross-sectional areas of the incident and transmission bars, respectively. The quantities ε_i and ε_r are the incident and reflected signals in the incident bar. The engineering strain is obtained from the time integration of the bar signals in Eq. 2. However, it is difficult to accurately measure strains in brittle materials using only the bar signals. Hence, DIC was also used to measure the strain history and strain rate of the specimen.

A typical example of the raw strain gage signals from a SHPB experiment on bone is shown in Fig. 4. A triangular-shaped incident pulse, such as the one shown in Fig. 4, is
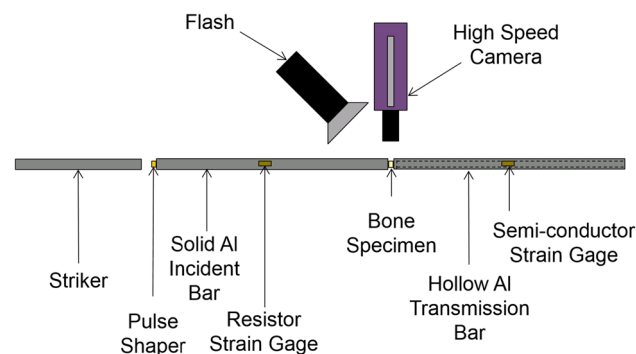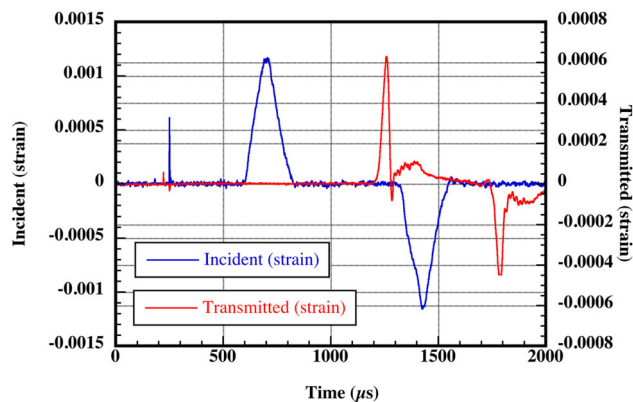

Fig. 4 Raw bar engineering strain signals from SHPB experiment on human cortical bone

typically used for high-rate experiments on brittle materials [23]. The incident bar pulse was shaped to increase the rise time to ensure that the bone specimen was in a state of dynamic equilibrium over the course of the experiment. Verification of dynamic equilibrium requires that the stress state is constant throughout the specimen; this is assumed when the force on both sides of the specimen are equal during the experiment, or $F_{front} = F_{back}$. The typical forces measured (or calculated) on either side of the specimen, shown in Fig. 5, verify that the front and back surface forces were approximately the same throughout the experiment. The force history calculated at the front surface (incident bar-specimen interface) is much noisier than the back surface (specimen–transmission bar interface) because of the higher signal-to-noise ratio of the hollow transmission bar and semiconductor gages in it, compared to the solid incident bar with resistive gages. Force at the input bar is calculated by subtracting the reflected signal from the incident signal, which are approximately of the same magnitude. This further amplifies noise and hence the
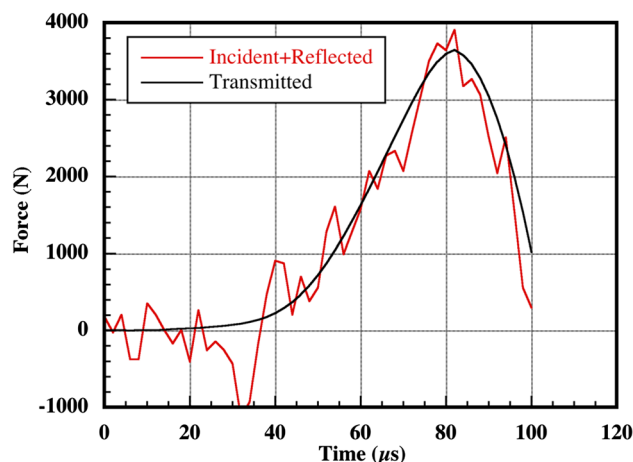

Fig. 3 Schematic of the compression split-Hopkinson bar set-up

Fig. 5 Dynamic equilibrium of cortical bone compression sample

fluctuation in the calculated force. Reduction of noise would improve equilibrium verification and could be achieved with the addition of semi-conductor gages to the incident bar. Even though the calculated force at the input bar interface shows large fluctuations, its average trend follows the output bar interface force.

In addition to being in dynamic equilibrium, the cortical bone specimen experienced an approximately constant rate of deformation after an initial ramp loading, as shown in typical strain and strain rate histories in Fig. 6. Figure 6 shows that after a strain acceleration time from about 10–40 μs, the strain rate becomes approximately constant from 40 to 80 μs, as the sample deformed at an approximate strain rate of between 1700 and 2000/s, using traditional bar signal analysis. The strain data shown in Fig. 6 follows the work by Frew et al. [35] on brittle materials, such as Macor and Indiana limestone. After 80 μs, the specimen begins to fail macroscopically. After failure initiation, there is little resistance to the motion of the incident bar, and after 80 μs, the data is no longer representative of the material response.

Measurement of small displacements of the bar ends is inaccurate because of slight variations in strain gage factor and the inability to prepare perfectly flat and parallel loading specimen surfaces. Elastic behavior is not reported for most materials using only bar signals; specimens with directly bonded strain gages or other techniques are necessary to accurately obtain the small strain mechanical response. For comparison, the bone specimen strain history is extracted using both DIC and the standard SHPB bar signal analysis for one experiment. Strain rate and strain (integrating strain rate) obtained from the bar signal are shown in Fig. 6. Figure 7 compares the strain data from the two techniques: surface strain from DIC and strain obtained from measured bar strains. The DIC strains were obtained in two different ways. DIC strain (mean) was
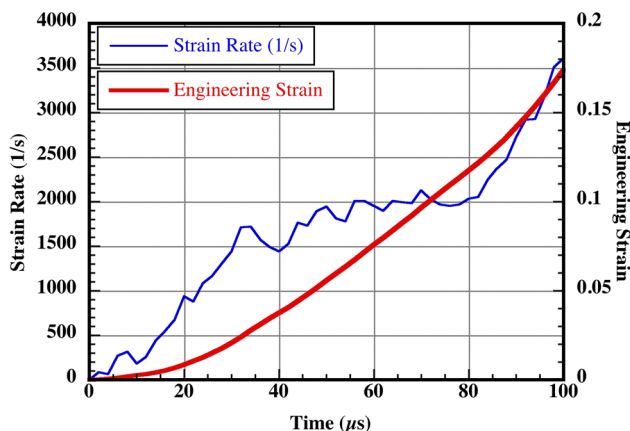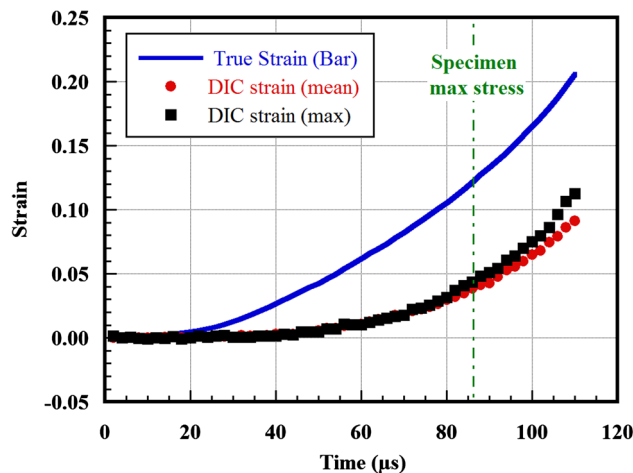

Fig. 7 Typical true strain histories from a dynamic (transverse) compression experiment using DIC and *bar* signal analysis

obtained by averaging the strain over the entire analyzed specimen surface area. The DIC strain (max) data is the largest magnitude of the measured DIC strain from the entire analyzed specimen surface area. As Fig. 7 shows, the DIC strain is much lower than the bar signal strain. There are two reasons for the difference in measurement between the two techniques. First, use of bar signals to measure small displacements is not accurate. This difference between the two techniques emphasizes the necessity for the use of strain gages or optical techniques to measure small strain deformation directly on the specimens. The bar signals are not accurate enough to measure the small displacements obtained in compression on relatively brittle materials. It is for this reason that, traditionally, material modulus is not obtained from bar signals alone.

The second reason for the difference is that there may be a slight gap between the specimen and one of the bars at the beginning of the experiment. This is due to the specimens not being perfectly flat and parallel. Additionally, due to the relatively low strength of the material, the authors did not want to pre-load the specimens by significantly compressing the bars together. It was preferred to leave a small gap to be taken up by the motion of the bar, since even hand compressing of the bars could generate forces of 200 + N. Since this "gap take-up" would contribute to specimen strain using bar signals and be ignored by the DIC strain measurement, this contributes to the difference between the two (and also explains why the bar strain begins to increase earlier than the DIC strain).

The maximum and average DIC strain values are nearly identical up to the maximum load at 85 μs. This indicates that the strain profile over the specimen is relatively uniform up to the maximum load. The two DIC curves diverge after maximum load as the specimen begins to crack or fail, and develops localized strain concentrations.
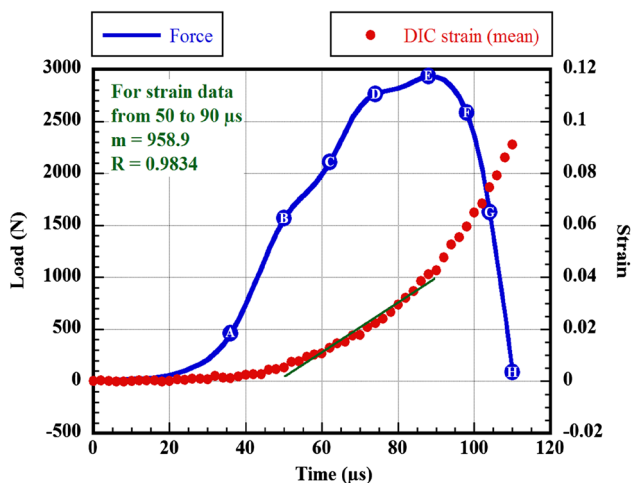

Fig. 6 Average engineering strain rate and strain histories of human cortical bone specimen at high rate using bar signals

Fig. 8 True strain (from DIC) and load histories for typical high rate compression experiment

The load and averaged DIC strain histories for the same experiment in Fig. 7 are shown in Fig. 8. Figure 8 shows that the strain history is not linear up to the max load during the experiment; however, the strain is approximately linear from half load (50 µs) to max load (90 µs). This indicates that the strain rate is approximately constant over the latter half of the experiment, achieved after the incident bar has been accelerated to a constant velocity. It is over this time range that the strain history was used to determine the strain rate of the experiment. For this experiment, the strain rate was approximately 960/s. After maximum load is reached, the specimen begins to fail and the strain rate increases.

The high-rate compression experiments were performed with 19.05 mm diameter bars and 4 × 3 mm specimens. The large diameter of the bars relative to the small dimensions of the specimens created blurred edges in the high-speed imaging due to the bar surface being closer to the optical lens than the focal plane. This limited the amount of axial length of the specimen that was available to be used in the DIC analysis to obtain strain measurements. Smaller diameter bars, such as 12.7 mm or even 6.35 mm, would reduce the blurriness since the bar surfaces would be closer to the focal plane of the camera and produce images where the area of interest for DIC analysis could extend closer to the specimen edges. Though a somewhat narrow area was used to obtain strain measurements, the strain is uniform across this area, indicating the validity of the high rate experimental technique. Figure 9 shows a series of images of a compression specimen with axial-strain contours, during the same high-rate experiment of the previous figures. The eight images (a–h) correspond to the blue point-markers on the load history in Fig. 8. Figure 9i shows the specimen after failure (displacement

contours are not present due to large discontinuous localized deformation). The strain contours in Fig. 9 show that after the maximum load is reached (e), strain begins to localize around cracks, leading to failure. Therefore, the strain data shown in Fig. 8 after maximum load is the averaged strain across the specimen, although there are points of higher strain due to localized deformation (see Fig. 7 for a comparison between averaged and maximum strain after peak load).

Results

Compressive Mechanical Response as a Function of Strain Rate and Orientation

The averaged mechanical response from the quasi-static (0.001/s), intermediate (1/s), and high-rate (1000/s) experiments are shown in Fig. 10 for both longitudinal and transverse orientations. Error bars in all plots represent ± 1 standard deviation ($\pm 1\sigma$). As the strain rate increased, the mechanical response was stronger and stiffer for both orientations. The longitudinal response was much higher at all strain rates than the transverse response. In addition, it was observed that the elongation to failure was much lower at the dynamic rate for the transverse orientation, indicating the bone became more brittle. In general, the transverse response had a longer flat plateau region corresponding to permanent irreversible deformation after ultimate stress at quasi-static and intermediate rates. This indicates that transverse specimens were more ductile, or perhaps the transversely loaded specimens possess a mechanism, such as increased micro-cracking, which allows for more irreversible deformation before failure. The longitudinal orientation did not show rate dependence on ductility, as the strain to failure over the range of strain rates was fairly constant. This constant value of strain to failure for the longitudinal loading was approximately the same as the strain to failure of the transverse loading at dynamic rate.

The ultimate strength (maximum stress) was found to be dependent on the strain rate for both loading directions. This relationship is linear when plotted on a semi-log scale, as shown in Fig. 11, meaning that the true relationship is exponential. The longitudinally loaded specimens exhibited a higher ultimate strength compared to transversely loaded specimens for all strain rates.

The data shows a high amount of scatter, which is not surprising because of the typical location to location variability and defects that are present in biological materials. This variability is most likely due to the presence of an appreciable number of natural differences in the bone specimens including: mineral content, microstructural flaws, variations in osteon size, and orientation of osteon
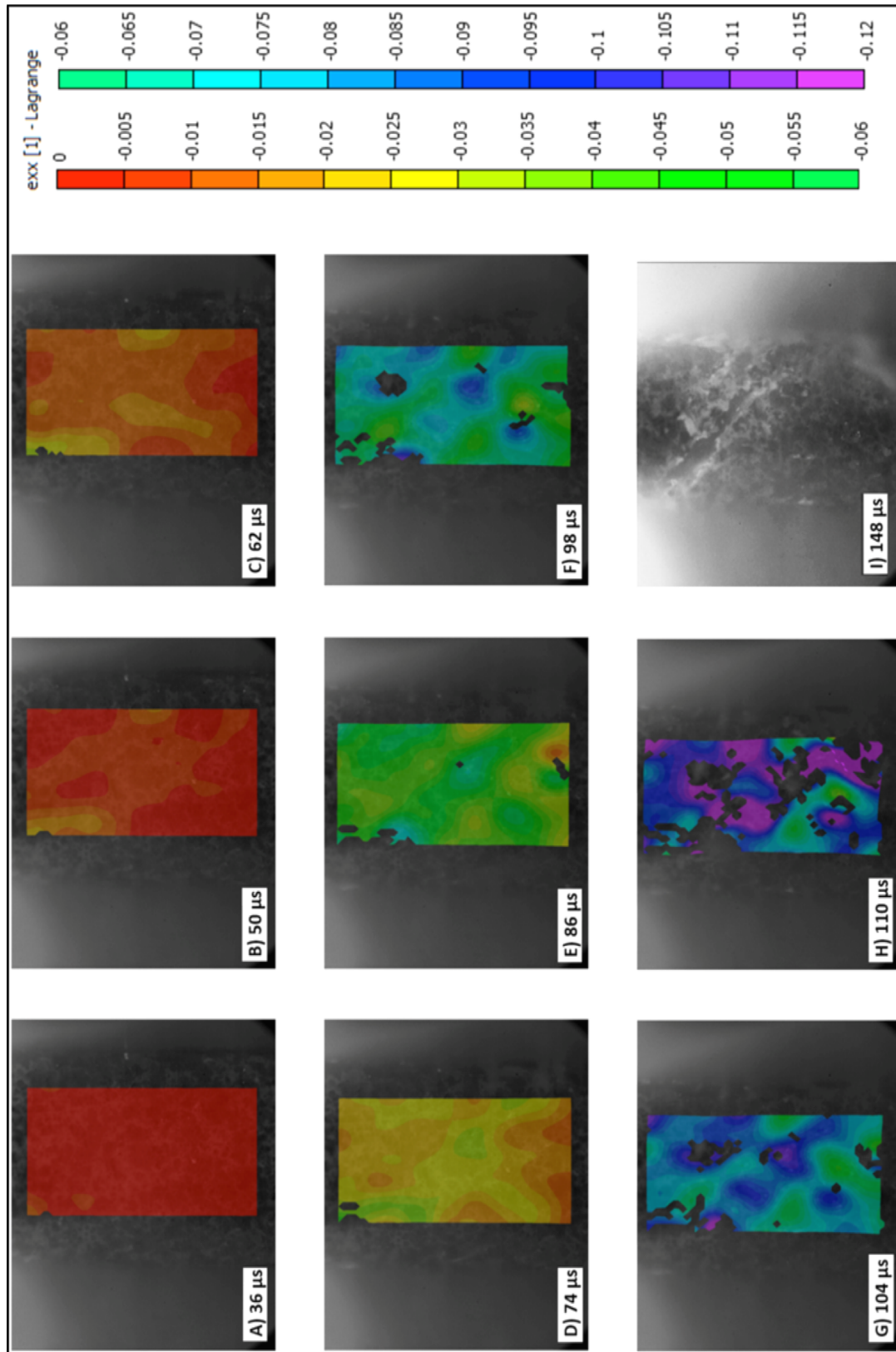
Fig. 9 High-rate images of the specimen during the experiment with DIC strain contours at times **a** 36 μs, **b** 50 μs, **c** 62 μs, **d** 74 μs, **e** 88 μs (max load), **f** 98 μs, **g** 104 μs, **h** 110 μs, and **i** 148 μs (fully failed). The length of the speckled bone in the photos is approximately 3–4 mm

82

J. dynamic behavior mater. (2016) 2:74–90

axes relative to the loading direction. However, as is shown in Fig. 11, the donor-to-donor variability is surprisingly low (all three donor averages are tightly grouped at each rate) considering the wide range of variables that contribute to bone strength.

Specimen location dependency (relative to location along the diaphysis or angular position) was not investigated. Conclusions regarding any correlation between age and compressive strength could not be made because of both the limited number of donors and the narrow age range of the donors (36–50 years) in this study.

In addition to ultimate strength, the average modulus (initial linear slope of the stress–strain plot) was also found to be loading rate dependent, as shown in Fig. 12. The average moduli of both the longitudinal and transverse samples increased linearly with strain rate when plotted on a semi-log scale, indicating an exponential behavior. The average modulus also depended on loading direction, with the longitudinally loaded specimens stiffer than the transversely loaded specimens.
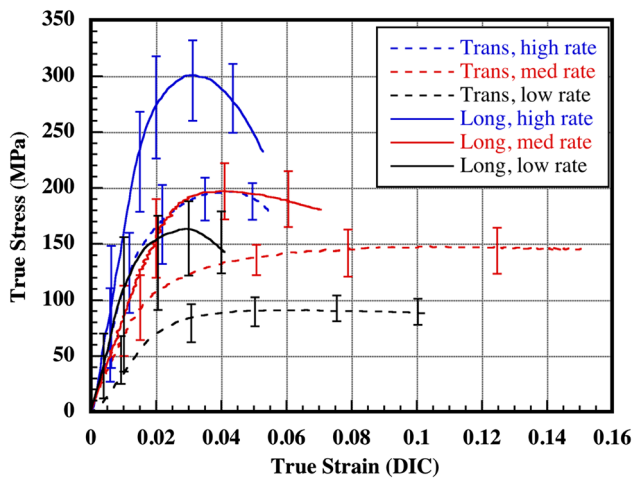
Fig. 10 Compressive mechanical response of human femoral cortical bone as a function of strain rate and loading orientation

Fig. 11 Ultimate compressive strength as a function of strain rate and loading orientation for individual donors and overall averages
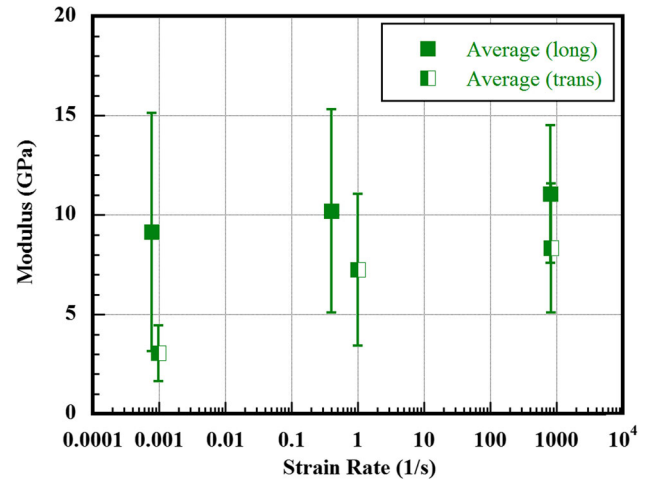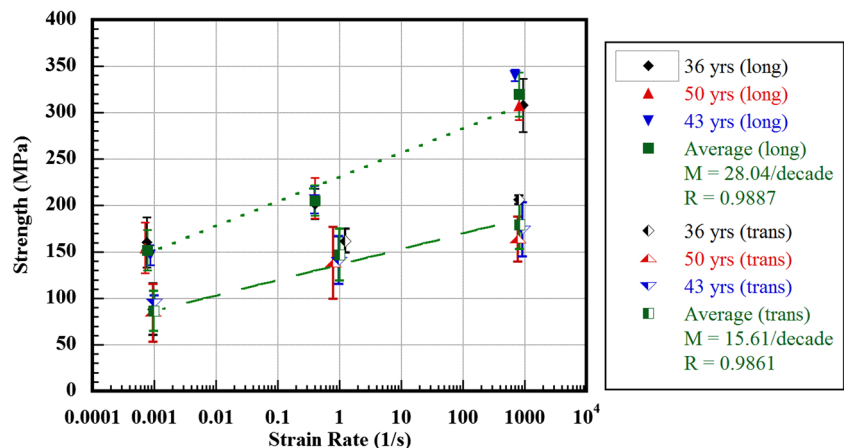
Fig. 12 Average elastic modulus as a function of strain rate and loading orientation

A summary of ultimate strain (strain at the maximum stress level) as a function of strain rate is shown in Fig. 13. The transversely loaded specimens reached a higher ultimate strain compared to the longitudinally loaded specimens at low and intermediate rates; however, at high rate the failure strains of the two directions approached the same range.

Discussion

A comprehensive summary of the strain rate dependent mechanical properties of cortical bone from this study and various other studies is given in Tables 2, 3, 4, 5. These tables also provide the method used in loading the specimens, test condition of the bone (dry, wet, or embalmed), and the strain measurement method, all of which are critical to the measured results. In addition, for high rate experiments, these tables also contain the status of dynamic
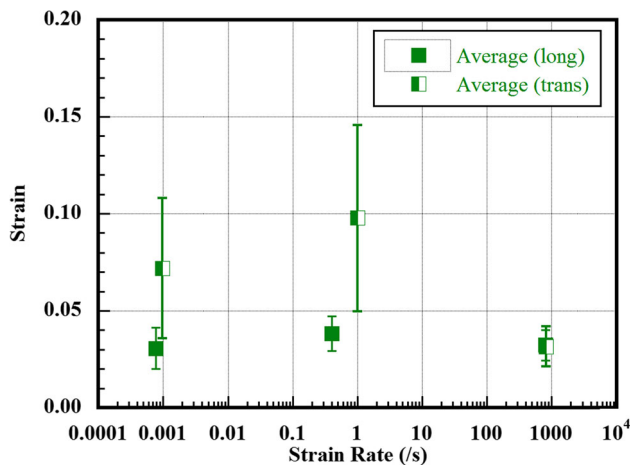
Fig. 13 Average ultimate strain as a function of strain rate and loading orientation

equilibrium, which must be verified for a valid high rate experiment. Empty cells indicate that the information was omitted in the original publication.

This paper demonstrates the importance of direct strain measurements. Far field strain measurements using machine displacement or bar signal analysis could introduce significant measurement error. The compressive properties of human cortical bone are summarized in Tables 2, 3 for loading in the longitudinal and transverse orientations, respectively. Tables 4, 5 provide similar data from animal studies. These tables are not exhaustive of all bone mechanical research, but include select studies where high strain rate response was investigated.

For comparison, the rate dependent compressive strength data from both human and animal studies are presented in Fig. 14, while corresponding Young's moduli are given in Fig. 15. In general, the compressive strength increases with strain rate for all species in both longitudinal and transverse loading directions. Transverse strengths are consistently lower than the corresponding longitudinal strengths for all strain rates. These trends are also apparent for elastic moduli.

The moduli measured in the present study were consistently lower than the other studies. This is surprising as the in situ DIC strain measurement provided lower strain values than the corresponding SHPB analysis, which increased the modulus values. If traditional bar analyses had been used, the moduli obtained here would have been even lower. This reinforces the necessity of accurate small strain measurement using DIC, strain gages or other direct techniques.

For the studies shown here, the compressive strength of large mammal femoral cortical bone is somewhat higher than human femoral cortical bone, as would be expected

due to the large disparity in body mass. As strain rate increases to dynamic, the large mammal advantage in strength becomes more pronounced. There appears to be less of an effect of species type on the modulus of cortical bone, as the moduli measured in human and animal studies overlap at all strain rates.

Comparison of Cortical Bone Studies

The compressive response found in this study agreed with other studies on human bones. McElhaney [7] found that embalmed human femur has an ultimate strength of 140 MPa at quasi-static rate, while the strength at high rate (1500/s) was 300 MPa in the longitudinal direction of the bone. In general, direct comparisons between embalmed and fresh bone are not recommended because of the significant effects of embalming on bone microstructure and its constituents, leading to altered bone mechanical properties [8]. In an attempt to quantify these effects, McElhaney et al. [8] conducted a comparative study and found that embalming caused a 12 % reduction in ultimate compressive strength. After the 12 % reduction in strength due to embalming was corrected, the range of ultimate strength found for human bone by McElhaney [7] would be 168–355 MPa, similar to the values found in this study.

Reilly and Burstein's [27] quasi-static strength of longitudinal human femur is similar to this study (193 compared to 152 MPa in this study). The compressive strength for the transverse direction, however, was found to be 132 MPa at quasi-static rate, compared to the average value of 86.6 MPa observed in this study.

Like human bone, bovine and equine bone strength measured by Adharapurapu et al. [18], Bekker et al. [20], and Kulin et al. [24], respectively showed rate dependence in compression and found that the behavior was linear with strain rate when plotted in a semi-log plot. Bovine and equine bones had higher ultimate stresses compared to the human bones used in this study, underscoring the necessity for human tissue studies at high strain rates, as these are the rates that are relevant to extreme dynamic environments when developing material response models to be used for numerical simulations of events where humans are involved. Figure 14 graphically shows the compressive strengths of several studies as a function of strain rate. The divergence of animal data from human data at high rate can be seen from this plot. The overall stress–strain *trends* of cortical bone measured in this study agree with bovine and equine studies in that the mechanical properties of the bone were anisotropic. Unfortunately, some investigators used dry bones for their studies, making it impractical to draw comparisons of the mechanical response to wet bones because of the significant effect of hydration of collagen on the mechanical behavior [14, 15].

84

J. dynamic behavior mater. (2016) 2:74–90

Table 2 Longitudinally loaded compression results on human cortical bones from various studies

Study	Material (D dry, E embalmed, W wet)	Test type (L longitudinal, T transverse)	Age (years) and sex (M male, F female)	Strain rate (s⁻¹)	Compressive strength max (MPa)	Elastic modulus (GPa)	Strain to failure (%)	Strain measurement method
Ko et al. [36]	Femur ( )	Low Strain Rate				17.3		
Sedlin et al. [37]		Bending				15.8		
McElhaney [7]	Femur (E)	Compression (L)	24 M	0.001	150.34	15.17	1.65	Piston velocity
			25 M	0.01	179.31	17.24	1.75	
			26 M	0.1	200.0	17.93	1.8	
			27 M	1	220.69	22.07	1.78	
			28 M	300	279.31	29.66	1.1	
			29 M	1500	317.24	40.69	0.95	
Abendschein et al. [38]	Femur ( )	Ultrasonic (L)			NA	29.5		
Bargren et al. [39]	Femur (W)	Compression (L)	23 M	0.052		15.94 ± 0.4		Strain gage
	Femur (D)	Compression (L)	23 M	0.052		18.91 ± 0.3		
Reilly et al. [27]	Femur (W)	Compression (L)	21 M	0.2–0.5	206 ± 10		1.9 ± 0.29	Extensometer
			22 M	0.2–0.5	211 ± 14.4		1.8 ± 0.07	
			31 M	0.2–0.5	203 ± 27.6		1.9 ± 0.34	
			52 M	0.2–0.5	198 ± 12.7		1.8 ± 0.38	
			Average	0.2–0.5	193		1.85	
Burstein et al. [40]	Femur (W)	Compression (L)	20–29 M and F	Low (~0.35)	209 ± 3.5	18.1 ± 0.28		Extensometer on specimen
			30–39 M and F		209 ± 8.5	18.6 ± 0.14		
			40–49 M and F		200 ± 17.0	18.7 ± 1.48		
			50–59 M and F		192 ± 16.8	18.2 ± 0.61		
			60–69 M and F		179 ± 14.9	15.9 ± 0.68		
			70–79 M and F		190 ± 19.6	18.0 ± 1.86		
			80–89 M and F		180	15.4		
			Femur Average		194	17.4		
	Tibia (W)		30–39 M and F		204	35.3		
			40–49 M and F		204 ± 7.6	30.6 ± 11.05		
			50–59 M and F		192 ± 0.5	24.5 ± 1.05		
			60–69 M and F		183 ± 6.0	25.1 ± 1.12		
			70–79 M and F		183	26.7		
			80–89 M and F		197	25.9		
			Tibia average		194	28.0		

J. dynamic behavior mater. (2016) 2:74–90

85

Table 2 continued

Study	Material (D dry, E embalmed, W wet)	Test type (L longitudinal, T transverse)	Age (years) and sex (M male, F female)	Strain rate (s⁻¹)	Compressive strength max (MPa)	Elastic modulus (GPa)	Strain to failure (%)	Strain measurement method
Smith et al. [41]	Femur (W)	Compression (L)	19–87 M and F	0.001	61.6 ± 4.9			None
Lappi et al. [42]	Femur (E)	Ultrasonic (L)				5.5		Strain gage
Katsamanis et al. [16]	Femur (E)	Compression ball bearing impact/SHPB (L)	45–55 M	0.00002 / 100		16.2 / 19.9		
Ohman et al. [43]	Femur and Tibia (W)	Compression (L)	4–15 / 22–61	0.1 / 0.1	104 / 194.4	12.47 / 17.7	2.31 / 1.84	Extensometer
This Study	**Femur (W)**	**Compression (L) Hydraulic instron**	**36–50 M**	**0.001 / 1**	**152.1 ± 21.6 / 205.3 ± 16.5**	**9.15 ± 5.98 / 10.2 ± 5.11**	**3.06 ± 1.06 / 3.83 ± 0.9**	**DIC on specimen (optical)**
		Compression (L) Hopkinson Bar		**1000**	**319 ± 23.9**	**11.05 ± 3.46**	**3.24 ± 0.79**	**DIC on specimen (optical) with dynamic equilibrium and constant strain rate**

Empty cells indicate that the information was not available in the original publication

Elastic Modulus

The modulus (slope of the initial part of the stress–strain curve) from this study was lower than moduli reported from other studies (Fig. 15; Tables 2, 3). The modulus of the bone in the longitudinal direction was 9.15 ± 5.98 GPa at quasi-static rates, while at dynamic rates the modulus was 11.05 ± 3.46 GPa. In the transverse direction, the modulus of the bone was 3.05 ± 1.14 GPa at quasi-static rate and 8.3 ± 3.25 GPa at high rate, averaging over the three donors. Reilly and Burstein [27] observed an orientation dependence on the modulus of cortical bone at quasi-static rate; the longitudinal modulus was 17.0 GPa, and the transverse modulus was 11.5 GPa. Ohman et al. [43] investigated the longitudinal compressive behavior of femur and tibia, and found a combined average compressive modulus of 17.7 GPa. The strain rate dependence on modulus in the current study also differed from published dynamic data. Katsimanis and Raftopolus [16] studied the rate-dependent modulus of human femoral cortical bone in the longitudinal direction and found values of 16.2 and 19.9 GPa at quasi-static and dynamic rates, respectively. A possible cause for this difference could be that Katsamanis and Raftopolus [16] used strain gages bonded to the surface of the bone, which included a 2-day drying period of the bones for strain gages to adhere to the surface. Despite this difference in Young's modulus, the rate of increase in modulus with strain rate was similar. The results of Katsamanis and Raftopolus [16] show a 23 % increase in modulus from quasi-static to dynamic rates, while the results from this study show an increase of 21 % over a similar range of strain rates.

Differences in the measured modulus could be due to preservation methods and moisture content of the specimens; several other investigators dried bones specimens for an extended period of time, which could have affected the measured stiffness. Choi et al. [44] investigated the modulus of human cortical bone from a tibia using a three-point bend arrangement and found a specimen size dependency on modulus. Specifically, the modulus for relatively large specimens defined as having a height larger than 500 μm was consistently found to be around 15 GPa. Once the specimen size decreased below 500 μm, the modulus dropped to 4.6–5.5 GPa for cortical bone, showing the influence of specimen microstructural effects [osteon diameter is around 200 μm]. Choi et al. [44] posited that the reduction in modulus is due to microstructural defects present in the bone. Essentially, as the specimen size drops and the size of the defects such as pores and channels remain constant, defects have a more profound effect on the measured modulus.

Modulus results from the human studies were consistent showing a linear increase in modulus as a function of

86

J. dynamic behavior mater. (2016) 2:74–90

Table 3 Transversely loaded compression response from various studies in literature for cortical human bones, including this study, at different loading rates

Study	Material (D dry, E embalmed, W wet)	Test type (L longitudinal, T transverse)	Age (years) and sex (M male, F female)	Strain rate (s⁻¹)	Compressive strength max (MPa)	Elastic modulus (GPa)	Strain to failure (%)	Strain measurement method
Reilly et al. [27]	Femur (W)	Compression (T)	31 M	0.2–0.5	151 ± 12.7		8.7 ± 2.48	Extensometer
			52 M	0.2–0.5	118 ± 13.6		2.8 ± 0.29	
			Overall Average		133			
This Study	**Femur (W)**	**Compression (T)**	**36–50 M**	**0.001**	**86.60 ± 21.7**	**3.05 ± 1.14**	**7.21 ± 3.61**	**DIC on specimen (optical)**
				1	**146.98 ± 27.53**	**7.24 ± 3.8**	**9.78 ± 4.79**	
		Hydraulic Instron						
		Compression (T)		**1000**	**178.90 ± 26.02**	**8.30 ± 3.25**	**3.17 ± 1.28**	**DIC on specimen (optical) with dynamic equilibrium and constant strain rate**
		Hopkinson Bar						

Empty cells indicate that the information was not available in the original publication

Table 4 Longitudinal compression response of animal cortical bones from various animal bone studies from literature

Study	Material (D dry, E embalmed, W wet)	Test type (L longitudinal, T transverse)	Age (years) and sex (M male, F female)	Strain rate (s⁻¹)	Compressive strength max (MPa)	Elastic modulus (GPa)	Strain to failure (%)	Strain measurement method
Kulin et al. [24]	Equine femur (W)	Compression (L)	0.5–28	0.001	173	14.07	1.35	Bar strain gages/machine disp dynamic equilibrium
		Hydraulic/ Hopkinson Bar		1	332	15.61	2.60	
				1000	528	33.95	1.90	
Adharapurapu et al. [18]	Bovine femur (W)	Compression (L)	Adult ("slaughter age")	0.001	165	8.41		Bar strain gages/machine disp dynamic equilibrium
		Hydraulic/ Hopkinson Bar		0.01	164	4.85		
				0.1	206	6.60		
				1	236	7.98		
				1000	458	16.23–36.90	2.58	
	Bovine Femur (D)			0.001	185	5.53		
				0.01	283	12.59		
				0.1	315	10.62		
				1	289	9.94		
				1000	557	20.52	2.72	
McElhaney [7]	Bovine Femur (W)	Compression (L)	Not specified	0.001	175	18.62	1.88	Piston velocity
		Pressurized air piston		0.01	207	20.00	1.82	
				0.1	231	24.14	1.75	
				1	252	27.59	1.25	
				300	283	33.11	1.00	
				1500	366	42.08	0.90	
Bekker et al. [20] Cloete et al. [19]	Bovine Femur (W)	Compression (L) Screw driven machine/ Hopkinson Bar constant strain rate	Not specified	0.0001	149.6 ± 13.7	3.74	3.98 ± 0.4	Slow rate machine disp/high rate Bar gages dynamic equilibrium
				0.001	171.9 ± 18.5	3.81	4.51 ± 0.4	
				0.01	202.1 ± 14.9	3.96	0.051 ± 0.4	
				0.1	234.8 ± 15.5	3.79	6.2 ± 0.2	
				250	383.9 ± 21.3	15.60	2.4 ± 0.3	
				1000	413.9 ± 28.7	15.33	2.7 ± 0.1	

Empty cells indicate that the information was not available in the original publication

Table 5 Transverse compression response of animal cortical bones from various animal bone studies from literature

Study	Material (D dry, E embalmed, W wet)	Test type (L longitudinal, T transverse)	Age (years) and sex (M male, F female)	Strain rate (s^{-1})	Compressive strength max (MPa)	Elastic modulus (GPa)	Strain to failure (%)	Strain measurement method
Kulin et al. [24]	Equine Femur (W)	Compression (T) Hydraulic/ Hopkinson Bar	0.5–28	0.001	119	9.65	0.016	Bar strain gages/machine disp dynamic equilibrium
				1	202	10.91	0.027	
				1000	320	15.82	0.0275	
Adharapurapu et al. [18]	Bovine Femur (W)	Compression (T) Hydraulic/ Hopkinson Bar	Adult ("slaughter age")	0.001	143	Not Specified		Machine disp
				0.01	141			
				0.1	155			
				1	195			
				1000	296	10.42	0.045	Bar strain gages/dynamic equilibrium
	Bovine Femur (D)			0.001	201	Not specified		Machine disp
				0.01	204			
				0.1	170			
				1	319			
				1000	363	12.03	0.0323	Bar strain gages/dynamic equilibrium

Empty cells indicate that the information was not available in the original publication

increasing log of strain rate. The studies conducted on bovine cortical bone by Adharapurapu et al. [18] and Bekker et al. [20] showed little variation in modulus at the low to intermediate strain rates (less than 250/s strain rate) and a significant increase in modulus as the rate increased to the dynamic range. At all strain rates, moduli data from Adharapurapu et al. [18] was always higher than that observed by Bekker et al. [20]. It is necessary to point out that in most of these experiments, strains are measured using either the Hopkinson bar calculations or from the loading machine, and not directly on the specimen.

Comparison of Mechanical Response of Tibia and Femur

The mechanical properties of the femur may not represent the mechanical behavior of other cortical bones in the leg or elsewhere. The compressive results from the present study seem to agree with Ohman et al. [43], who found the compressive strength of an adult bone to be 191.4 MPa. However, they mixed femur and tibia specimens and presented them as a single average value. Furthermore, a study comparing tibia bone material properties to those of the femur found a similar range of values for the ultimate strength of both bones at low strain rates [40]. However, the stiffness of the tibia was noted to be 34–90 % higher

than the stiffness of femur, concluding that the mechanical properties of the femur and tibia are different and should not be grouped together as one material. This finding was consistent with similar comparison studies on the mechanical properties of the femur and tibia [36, 45, 46]. Burstein et al. [40] also showed that femoral tissue undergoes degradation in all mechanical properties with age, while tibial tissue only shows an increase in ultimate strain.

The mechanical properties of bone differ not only throughout the body, but also within any specific bone [47, 48]. Studies of the mechanical properties show that the properties of the subchondral bone of the femoral head [49] (the metaphyseal section), which is located between the diaphysis and the epiphysis in the proximal femur, are different from the properties of the diaphysis [50]. Regarding the tibia bone, the metaphyseal [51] and subchondral [44] bones in the proximal tibia have been shown to have properties of lower magnitude in comparison to the diaphyseal bone. Because of the differences in the mechanical properties of the femur and tibia, the use of a single value of yield strength, ultimate strength, or modulus for femur and tibia would be inappropriate. Orais et al. [48] found that the degree of anisotropy also varied along the length of the femur diaphysis. Therefore, when developing a high-fidelity computational model of a human anatomy,
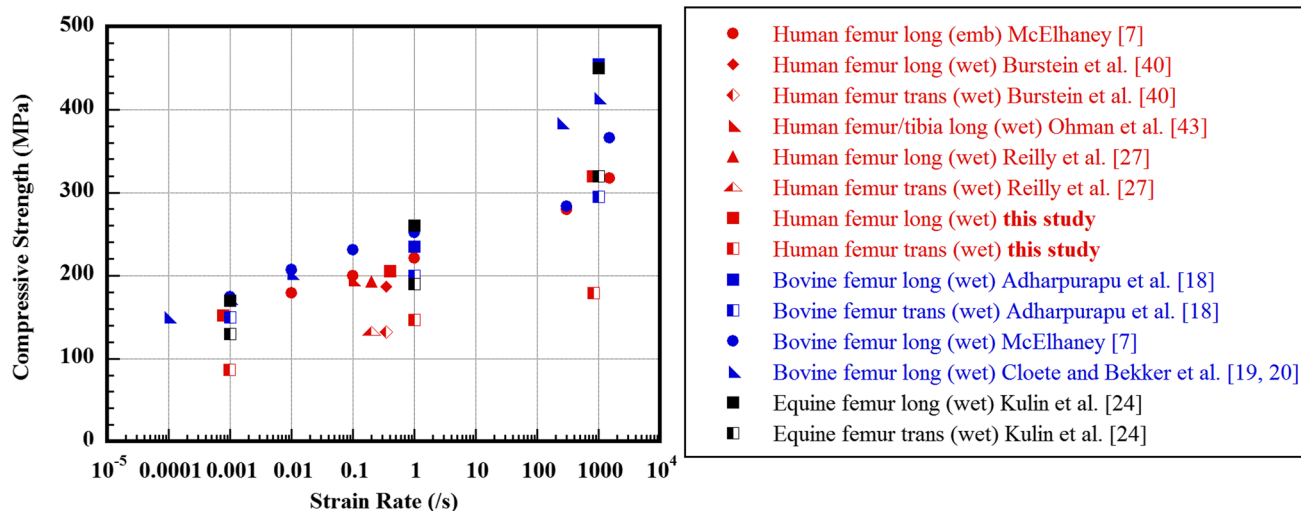
88

J. dynamic behavior mater. (2016) 2:74–90

Fig. 14 Compressive strength of cortical bone as a function of strain rate from various studies
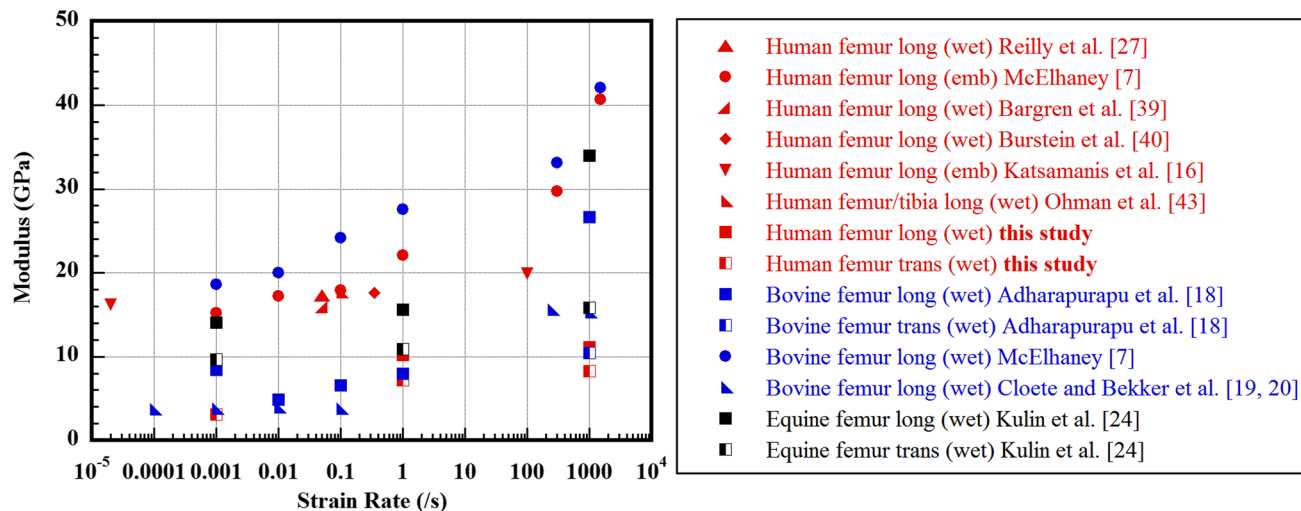

Fig. 15 Compressive elastic modulus of cortical bone as a function of strain rate from various studies

each type of bone must be studied separately to obtain its specific material properties.

Summary

A uniaxial compressive study of human femoral cortical bone was completed over a range of strain rates from quasi-static (0.001/s) to high rates ($\sim$1000/s). Loading was applied in the transverse and longitudinal directions of the bone axis. An Instron hydraulic load frame was used for quasi-static and intermediate rate (1/s) experiments while a SHPB setup was used for high-rate experiments. Optical strain measurements were performed using DIC with a variety of cameras, depending on the strain rate.

The ultimate strength and modulus were found to be anisotropic, where the longitudinal direction was both stronger and stiffer than the transverse direction. Ultimate strength and modulus increased with increasing strain rate while ultimate strain was constant for longitudinal specimens and depended on strain rate for transverse specimens. The compressive response measured in this study agreed with other studies on human bones.

Any correlations based on the specimen harvest location could not be concluded from this study with the limited sampling size, even though differences in strength, moduli, and hardness have been shown to vary with specimen location along the femur shaft (diaphysis) as well as at the ends (epiphysis). Conclusions about the relationship of age to ultimate compressive strength or stiffness could not be

made due to the narrow age range of the donors in this study.

Mechanical properties of the femur should not be applied to other bones for numerical modeling purposes, especially in the case of the tibia, which has been found to have different failure strengths and moduli compared to the femur. Further work is needed to quantify rate-dependent regional variations within the same bone. Additional studies are needed to assess the relationship between possible changes of failure strength with donor age or microstructural details such as osteon density and diameter, mineral content and porosity.

References

1. Ritchie RO, Kinney JH, Kruzic JJ, Nalla RK (2005) A fracture mechanics and mechanistic approach to the failure of cortical bone. Fatigue Fract Eng Mater Struct 28:345–371

2. Zimmermann EA, Schaible E, Bale H, Barth HD, Tang SY, Reichert P, Busse B, Alliston T, Ager JWIII, Ritchie RO (2011) Age-related changes in the plasticity and toughness of human cortical bone at multiple length-scales. Proc Natl Acad Sci 108:14416–14421

3. Launey ME, Buehler MJ, Ritchie RO (2010) On the mechanistic origins of toughness in bone. Annu Rev Mater Res 40:25–53

4. Gunnarsson CA, Sanborn B, Foster M, Moy P, Weerasooriya T (2012) Initiation fracture toughness of human cortical bone as a function of loading rate. In: Proceedings of the SEM international conference and exposition on experimental and applied mechanics, Costa Mesa

5. Sanborn B, Gunnarsson CA, Foster M, Weerasooriya T (2015) Quantitative visualization of human cortical bone mechanical response: studies of the anisotropic compressive response and fracture behavior as a function of loading rate. Exp Mech. doi:10.1007/s11340-015-0060-y

6. Shannahan L, Weerasooriya T, Gunnarsson CA, Sanborn B, Lamberson L (2015) Rate-dependent fracture modes in human femoral cortical bone. Int J Fract 194:81–92. doi:10.1007/s10704-015-0035-0

7. McElhaney J (1966) Dynamic response of bone and muscle tissue. J Appl Physiol 21:1231–1236

8. McElhaney J, Fogle J, Byars E, Weaver G (1964) Effect of embalming on the mechanical properties of beef bone. J Appl Physiol 19(6):1234–1236

9. Ohman C, Dall'Ara E, Baleani M, Van Sint Jan S, Viceconti M (2008) The effects of embalming using a 4% formalin solution on the compressive mechanical properties of human cortical bone. Clin Biomech 23:1294–1298

10. Sanborn BS, Gunnarsson CA, Foster M, Moy P, Weerasooriya T (2014) Effect of loading rate and orientation on the compressive response of human cortical bone. US Army Research Laboratory ARL-TR-6907

11. Tennyson RC, Ewert R, Niranjan V (1972) Dynamic Viscoelastic Response of Bone. Exp Mech 12:502–507

12. Lewis JL, Goldsmith W (1973) A biaxial split hopkinson bar for simultaneous torsion and compression. Rev Sci Instrum 44:811–813

13. Lewis JL, Goldsmith W (1975) The dynamic fracture and pre-fracture response of compact bone by split Hopkinson bar methods. J Biomech 8:27–40

14. Ntim MM, Bembey AK, Ferguson VI, Bushby AJ (2006) Hydration effects on the viscoelastic properties of collagen. MRS Proc 898E:39–43

15. Yamashita J, Furman BR, Rawls HR, Wang X, Agrawat CM (2001) The use of dynamic mechanical analysis to assess viscoelastic properties of human cortical bone. J Biomed Mater Res 58:47–53

16. Katsamais F, Raftopoulos D (1990) Determination of mechanical properties of human femoral cortical bone by the hopkinson bar stress technique. J Biomech 23(11):1173–1184

17. Tanabe Y, Tanaka S, Sakamoto M, Hara T, Takahashi H, Koga Y (1991) Influence of loading rate and anisotropy of compact bone. J Phys III 1(C3):305–310

18. Adharapurapu RR, Jiang F, Vecchio KS (2006) Dynamic fracture of bovine bone. Mat Sci Eng C 26:1325–1332

19. Cloete TJ, Paul G, Ismail EB (2015) Hopkinson bar technique for the intermediate strain rate testing of bovine cortical bone. Philos Trans R Soc Lond A 372:20130210

20. Bekker A, Cloete TJ, Chinsamy-Turan A, Nurick GN, Kok S (2015) Constant strain rate compression of bovine cortical bone on the split-Hopkinson pressure bar. Mater Sci Eng C 46(1):443–449

21. Ferreira F, Vaz MA, Simoes JA (2006) Mechanical properties of bovine cortical bone at high strain rate. Mater Charact 57:71–79

22. Lee OS, Park JS (2011) Dynamic deformation of bovine femur using SHPB. J Mater Sci Technol 25(9):2211–2215

23. Chen W, Song B (2010) Split Hopkinson (Kolsky) bar. Springer, New York, pp 29–77

24. Kulin RM, Jiang F, Vecchio KS (2011) Effects of age and loading rate on equine bone failure. J Mech Behav Biomed 4:57–75

25. Parish A, Chen W, Weerasooriya T (2009) High strain rate tensile behavior of pig bones. In: DYMAT 2009—9th international conference on the mechanical and physical behaviour of materials under dynamic loading, Brussels, vol 1, pp 917–922

26. Herwig K (2010) high rate properties of porcine skull bone tissue. Master's Thesis Purdue University, West Lafayette

27. Reilly DT, Burstein AH (1975) The elastic and ultimate properties of compact bone tissue. J Biomech 8(6):393–405

28. Martin RB, Burr DB (1998) Skeletal tissue mechanics. Springer, New York

29. Gustafson MB, Martin RB, Gibson V, Storms DH, Stover SM, Gibeling J, Griffin L (1996) Calcium buffering is required to maintain bone stiffness in saline solution. J Biomech 29(9):1191–1194

30. Chu TC, Ranson WF, Sutton MA, Peters WH (1985) Applications of digital-image-correlation techniques to experimental mechanics. Exp Mech 25(3):232–244

31. Sutton MA, Wolters WJ, Peters WH, Ranson WF, McNeill SR (1983) Determination of displacements using an improved digital image correlation method. Image Vis Comput 1(3):133–139

32. Bruck HA, McNeill SR, Russell SS, Sutton MA (1989) Use of digital image correlation for determination of displacements and strains. In: Workman GL (ed) Non-destructive evaluation for aerospace requirements. Gordon and Breach Science Publishers, Philadelphia

33. Sutton MA, McNeill SR, Helm JD, Schreier H (1999) Full-field non-contacting measurement of surface deformation on planar or curved surfaces using advanced vision systems. In: Proceedings of the international conference on advanced technology in experimental mechanics, July 1999

34. Chen W, Zhang B, Forrestal MJ (1999) A split Hopkinson bar technique for low impedance materials. Exp Mech 39:81–85

35. Frew DJ, Forrestal MJ, Chen W (2002) Pulse shaping techniques for testing brittle materials with a split Hopkinson pressure bar. Exp Mech 42:93–106

36. Ko R (1953) The tension test upon the compact substance of long bones of human extremities. J Kyoto Pref Med Univ 53:503–525

37. Sedlin ED (1965) A rheological model for cortical bone. Acta Orthop Scand 83:1–78

38. Abendschein W, Hyatt GW (1970) Ultrasonics and selected physical properties of bone. Clin Orthop Relat Res 69:294–301

39. Bargren JH, Bassett CAL, Gjelsvik A (1974) Mechanical properties of hydrated cortical bone. J Biomech 7:239–245

40. Burstein AH, Reilley DT, Martens M (1976) Aging of bone tissue: mechanical properties. J Bone Joint Surg 58(1):82–86

41. Smith B, Smith DA (1976) Relations between age, mineral density and mechanical properties of human femoral compacta. Acta Orthop Scand 47:496–502

42. Lappi VG, King MS, LeMay I (1979) Determination of elastic constants for human femurs. J Biomech Eng 101:193–197

43. Ohman C, Baleani M, Pani C, Taddei F, Alberghini M, Viceconti M, Manfrini M (2011) Compressive behavior of child and adult cortical bone. Bone 49:769–776

44. Choi K, Kuhn JL, Ciarelli MJ, Goldstein SA (1990) The elastic moduli of human subchondral, trabecular, and cortical bone tissue and the size-dependency of cortical bone modulus. J Biomech 23(11):1103–1113

45. Evans FG (1970) Mechanical properties and histological structure of human cortical bone; ASME70-WA/BHF-7. American Society of Mechanical Engineers, New York

46. Yokoo S (1952) The compression test upon the diaphysis and the compact subastance of the long bones of human extremities. J Kyoto Pref Med Univ 51:291–313

47. Evans FG, Lebow M (1951) Regional differences in some of the physical properties of human femur. J Appl Phys 3(9):563–572

48. Orais AAE, Deuerling JM, Landrigan MD, Renaud JE, Roeder RK (2009) Anatomic variation in the elastic anisotropy of cortical bone tissue in human femur. J Mech Behav Biomed 2:255–263

49. Brown TD, Vrahas MS (1984) The apparent elastic modulus of the juxtarticular subchondral bone of the femoral head. J Orthop Res 2(1):32–38

50. Lotz JC, Gerhart TN, Hayes WC (1991) Mechanical properties of metaphyseal bone in the proximal femur. J Biomech 24(5):317–329

51. Murray RP, Hayes WC, Edwards WT, Harry JD (1984) Mechanical properties of the subchondral plate and the metaphyseal shell. In: Transactions of the 30th orthopedic research society meeting, Atlanta, 6–9 February 1984, p 197